

ORIGINAL PAPER

Monochromatic aberrations and characteristics of retinal image quality

D Robert Iskander PhD

Michael J Collins PhD FAAO

Brett Davis BAppSc

Leo G Carney PhD FAAO

Contact Lens and Visual Optics

Laboratory, Centre for Eye Research,

School of Optometry, Queensland

University of Technology

Background: Patients use a wide variety of terms to describe the characteristics of their vision. These descriptions encompass the effects of their eyes' monochromatic aberrations.

Methods: To illustrate the effect of monochromatic aberrations on the quality of the retinal image, we mathematically reconstructed the image falling on the retina. This has been achieved by combining the properties of various scenes with the optical characteristics of the eye.

Results: The effects of some common monochromatic aberrations are illustrated. We also show examples of the retinal image characteristics for two eyes, one with a decentred corneal apex and a second with a decentred refractive surgery ablation.

Conclusions: The image reconstruction technique provides a powerful tool for investigating the quality of the retinal image. It provides the capacity for clinicians to better understand a patient's visual performance. The image reconstruction technique can also broaden our knowledge of the effects of various forms of aberrations on retinal image quality for complex real-world scenes.

(*Clin Exp Optom* 2000; 83: 6: 315–322)

Accepted for publication: 20 December 2000

Key words: monochromatic aberrations, pupil function, retinal image quality

When optometrists ask patients to describe their vision, they are presented with a wide array of responses that can include blurred, doubled, ghosted, smeared, distorted, washed-out and many variations on these themes. Within these varied descriptions of visual quality, lies significant information about the optical defects of the eye.

The image characteristics associated with the common refractive errors, such as spherical defocus and astigmatism, are well known. Defocus will cause the image to blur in an even, symmetrical fashion, whereas astigmatism will cause blurring primarily along one meridian. Measurements of the optical characteristics of the eye show that,

while defocus and astigmatism are the major aberrations, there are also higher order aberrations such as coma and spherical aberration present in most eyes.¹ The unique interaction between these higher and lower order aberrations in an individual eye gives rise to the distinctive nature of individual reports of vision quality.

Real-world scenes are complex in terms of their constituent spatial frequencies, contrast and the orientation of spatial detail. However, it is possible to break down the complexity of any scene (object), through traditional image processing techniques such as Fourier analysis, into its constituent spatial frequency and

contrast components. If the wavefront aberrations and the properties of the pupil are known, it is possible to mathematically simulate the retinal image of the eye in question by combining the object (scene) properties with the pupil function of the eye (derived from the wavefront aberration and amplitude pupil functions).

The optical properties of the eye can be characterised by the wavefront error function, which can be described by a polynomial series. The lower-order terms of this polynomial represent aberrations such as prism, defocus and astigmatism and are typically corrected by conventional means such as spectacles or contact lenses. The

higher order terms such as primary coma or primary spherical aberration are more difficult to correct.

The wavefront aberrations of the eye can be measured by a variety of techniques. The most widely-used techniques that are currently in use include the aberroscope,^{1,3} the Hartmann-Shack wavefront sensor,^{4,5} psychophysical methods^{6,7} and double-pass methods.^{8,9} There is growing interest in the effects of these aberrations as attempts are made to correct them for the purpose of improving acuity and to allow better observation of the retina.

The amplitude pupil function that is required to calculate the simulated retinal image is represented by both the pupil diameter and the transmittance of light through the various regions of the pupil. In 1933, Stiles and Crawford¹⁰ established in their seminal paper that light entering the eye through the edge of the pupil is less effective in eliciting a visual response than light entering through the centre of the pupil (the Stiles-Crawford effect). This effect has been shown to result predominantly from the orientation of photoreceptors, which align themselves with the centre of the pupil.¹⁰ To simulate the optical consequences of the directional nature of photoreceptors, the Stiles-Crawford effect can be represented as a filter in the plane of the pupil, which is darker towards the edge of the pupil and lighter towards the centre (so called apodisation).

In this paper, we present a method for reconstructing the retinal images based on monochromatic aberrations of the eye and pupil characteristics. We examine the effects of lower- and higher-order monochromatic aberrations on the qualities of the retinal image, to provide optometrists with a better understanding of the subjective descriptions of vision that their patients report. We also apply the method to the aberration data from subjects with a range of significant higher-order aberrations.

METHODS

Assumptions

The following analysis of the effects of monochromatic aberrations on the qual-

ity of the retinal image is based on several simplifications and assumptions. The modelling of visual performance which we have undertaken is based on monochromatic light (with $\lambda = 555$ nm) and takes no account of the contribution of the chromatic aberrations of the eye. We have omitted also the effects of light scatter within the media and retina. The image reconstruction only pertains to on-axis, foveal visual performance without any modelling of off-axis peripheral vision.

We have made the assumption that the retinal light image is what the person actually sees. However, this obviously ignores the role of neural processing in vision. For most eyes there should be a close correlation between the quality of the retinal image and vision performance, but in cases such as amblyopia, such an assumption is not correct.

Image reconstruction algorithm

The relationship between the input object, denoted in the Cartesian coordinates as $i(x,y)$, and the resulting output retinal image, $o(x,y)$, is given by the convolution integral

$$o(x,y) = \iint h(x-\tau_1, y-\tau_2) i(x,y) d\tau_1 d\tau_2 \quad (1)$$

where $h(x,y)$ denotes the point spread function (PSF). Note that both the input object and the PSF must have the same physical dimensions. The Fourier (spatial frequency) domain representation of the above relationship is given by

$$O(u_1, u_2) = H(u_1, u_2) I(u_1, u_2) \quad (2)$$

where $I(u_1, u_2)$, $O(u_1, u_2)$, and $H(u_1, u_2)$ are two-dimensional Fourier transformations of $i(x,y)$, $o(x,y)$, and $h(x,y)$, respectively. These transformations are with respect to x and y . The Fourier representations $I(u_1, u_2)$, $O(u_1, u_2)$, and $H(u_1, u_2)$ are often called object intensity spectrum, image intensity spectrum, and optical transfer function (OTF), respectively. The co-ordinates u_1 and u_2 denote the spatial frequencies in the x and y direction, respectively.

To link the optical properties of the eye, usually derived from the geometrical optics and Fourier theory, the concept of the

so-called pupil function (PF) has been introduced.¹¹ The PF, which uniquely characterises a linear optical system, has an analytic form given by

$$P(x,y) = A(x,y) \exp\{j2\pi W(x,y)\} \quad (3)$$

where $A(x,y)$ is the amplitude transmittance pupil function (Stiles-Crawford function), $W(x,y)$ is the wavefront error function, and $j = \sqrt{-1}$. The wavefront error function is usually defined as the difference between the optical path lengths of the ray under consideration and the chief ray scaled by the inverse of the wavelength.¹²

The PSF in (1) is necessary for the retinal image reconstruction and can be derived from the PF, defined in (3), as

$$h(x,y) = C \left| \iint P(x'y') \exp\{-j2\pi(xx' + yy')\} dx' dy' \right|^2 \quad (4)$$

where C is a normalisation factor that depends on the optics of the system, the wavelength and the radiant flux entering the pupil. This normalisation constant is omitted in our algorithm. We choose to normalise the resulting output retinal image to ensure that the image intensity ranges from zero to 255 (a grey scale image). The integral in (4) is essentially a magnitude square of a two-dimensional Fourier transformation of the PF with respect to x' and y' .

The image reconstruction algorithm can be summarised as follows. The preliminary step involves the objective measurement of the wavefront error function and the pupil transmittance function. It is important to note that such measurements are valid only for a fixed accommodation level.^{3,13} Next, a PF is formed and a two-dimensional Fourier transformation is used to calculate the PSF. For computer implementation, it is preferred to reconstruct the retinal image in spatial frequency domain using equation (2) and then inverse Fourier transform it back into space domain. These steps are evaluated by means of the so-called fast Fourier transform (FFT), the routines for which are available in most programming and simulation languages. It should be noted

that the object image and the PSF must have the same physical dimensions for the reconstruction algorithm to provide a meaningful result.

Modelling the pupil function

When accommodation is fixed, the wavefront error function can be represented in terms of Seidel series expansion or a finite series of Taylor or Zernike polynomials.^{14,15} The latest representations have become popular among vision researchers. However, care should be taken when comparing the results of different authors because there are several different classifications of Zernike polynomials.¹⁵

Mapping relationships exist between the first 15 Taylor and the first 15 Zernike coefficients¹ and an inverse relationship can easily be derived. Also mapping is available from Seidel to Zernike coefficients and vice versa.^{16,17} Although, in theory, all of these wavefront error expansions are equivalent, the Zernike polynomials seem to be the most suitable for accurate estimation of the wavefront error, due to their properties of orthogonality (that is, each term of the polynomial is independent of all other terms) and that fitting can be performed using the method of least squares that is linear in parameters.¹⁸

The Zernike polynomials can be described as a two-indexed function of radial and azimuthal frequency as¹⁵

$$Z_n^m(\rho, \theta) = \begin{cases} N_n^m R_n^m(\rho) \cos m\theta; & \text{for } m \geq 0 \\ -N_n^m R_n^m(\rho) \sin m\theta; & \text{for } m < 0 \end{cases} \quad (5)$$

where $N_n^m = \sqrt{2(n+1)/(1+\delta_{m0})}$ is the normalisation coefficient with δ_{m0} being a Kronecker delta function, R_n^m is a polynomial function given by

$$R_n^m(\rho) = \sum_{s=0}^{(n+|m|)/2} \frac{(-1)^s (n-s)!}{s! [0.5(n+|m|)-s]! [0.5(n-|m|)-s]!} \rho^{n-2s} \quad (6)$$

and (ρ, θ) are polar co-ordinates. From (5) and (6), it is clear that the index n describes the order of radial polynomial, while the index m describes the azimuthal

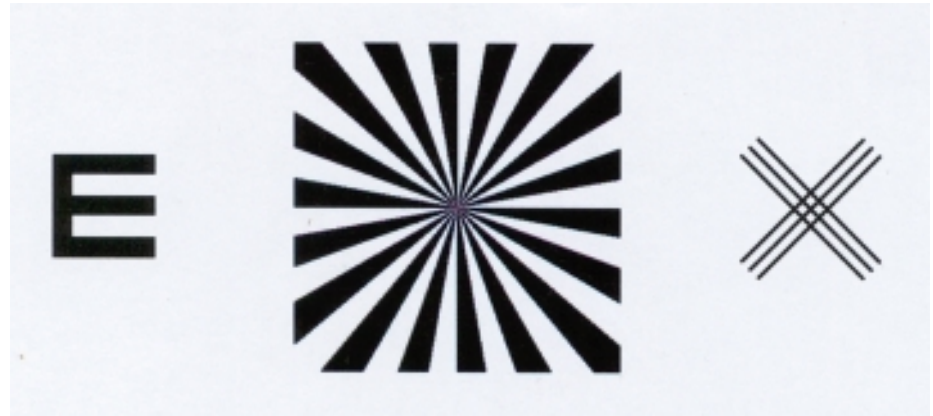


Figure 1. The original digital scenes used for evaluation of the algorithm for retinal image reconstruction

frequency of the sinusoidal component.

To derive the complete PF, we also need to model the second major variable, the amplitude transmittance pupil function. During accommodation, the pupil may change its size, shape or location.¹⁹ For a fixed accommodation level, the amplitude transmittance function is typically chosen to be modelled by a circular function or by a Stiles-Crawford function,²⁰ such as,

$$A(x,y) = \eta_{\max} 10^{[\rho_x(x-x_{\max})^2 + \rho_y(y-y_{\max})^2]} \quad (7)$$

where η_{\max} is the peak of sensitivity, ρ_x and ρ_y are the shape factors, and (x_{\max}, y_{\max}) are Cartesian co-ordinates of the peak. The Stiles-Crawford function models the directionality of photoreceptors in the human eye. It can be measured by psychophysical or reflectometric methods.^{21,22}

Test scenes used in the analysis

We have illustrated the effects of the lower- and higher-order monochromatic aberrations on the quality of the retinal image. For this purpose, we have selected three digital scenes shown in Figure 1. Each digital scene constitutes 256 by 256 pixels. Square images were chosen to simplify the computer implementation of the routines. A letter, a fan chart and a multiple cross are popular clinical methods of assessing vision. In those images, we have a variety of spatial frequencies. Each image

was assumed to be 50 mm by 50 mm and positioned six metres from the pupil plane. This corresponds to about one degree of visual angle.

It should be re-emphasised at this point that the monochromatic aberrations being modelled in this paper are on the visual axis and represent the aberrations occurring at the fovea. All of the scenes that we are depicting represent a visual angle, which is normally greater than that subtended by the fovea. The aberrations in the periphery of the eye are generally far greater than those on the visual axis but we have not attempted to simulate these peripheral aberration effects.

RESULTS

First, we show the effect of certain monochromatic aberrations on the retinal image quality. Each of these aberrations is represented by a single term of a finite Zernike series of radial order four. This means that, in our analysis, we have 15 different Zernike terms, which could be indexed from zero to 14. For the relationship between single and double indexing see the work of the VSIA.¹⁵ Through the paper, we have chosen a normative Stiles-Crawford function from the data²⁰ as a pupil transmittance function, unless otherwise stated. All the analyses are performed for a 6 mm pupil diameter

unless otherwise specified and the wavelength is set to 555 nm. The Zernike coefficients representing the wavefront are in units of wavelength. The refractive power maps are calculated from the wavefront assuming that the reference sphere is centred at the circle of least confusion. They are derived by constructing a surface that, when ray traced, would correspond to a given wavefront.

The effect of lower-order aberrations

In most classifications, the first six Zernike terms are assigned as lower-order terms. In our evaluation, we omit the first three. The zero Zernike term, $Z_0^0(\rho, \theta)$, represents piston, which by itself does not have any effect on the resulting retinal image. However, in conjunction with other terms the piston can be an important factor that balances the wavefront error function. The first and second Zernike terms, $Z_1^1(\rho, \theta)$ and $Z_2^1(\rho, \theta)$, represent horizontal and vertical prism, respectively. They cause a phase shift of the PSF and a subsequent shift of the retinal images. In practical terms, prism does not cause any loss in modulation transfer function (MTF) or vision in monocular conditions, as the eye simply alters its angle of gaze to align the point of interest in the scene with the fovea.

The third and fifth Zernike terms, $Z_2^2(\rho, \theta)$ and $Z_4^2(\rho, \theta)$, represent a 45- and a zero-degree primary astigmatism, respectively. It should be noted that the well-known astigmatism defined by Seidel corresponds not only to the third or fifth Zernike term but also to the combination of these terms with balancing defocus (fourth term) and piston. The retinal image affected by the balanced third Zernike term shows smearing along 45 degrees, as shown in Figure 2 together with the corresponding wavefront error function, the PSF and the refractive power map. Similarly, the retinal image affected by the balanced fifth Zernike term shows smearing along zero degrees. In real eyes, astigmatism is usually described by a combination of the third and fifth Zernike terms balanced by the defocus and piston terms.

The fourth Zernike term, $Z_3^0(\rho, \theta)$,

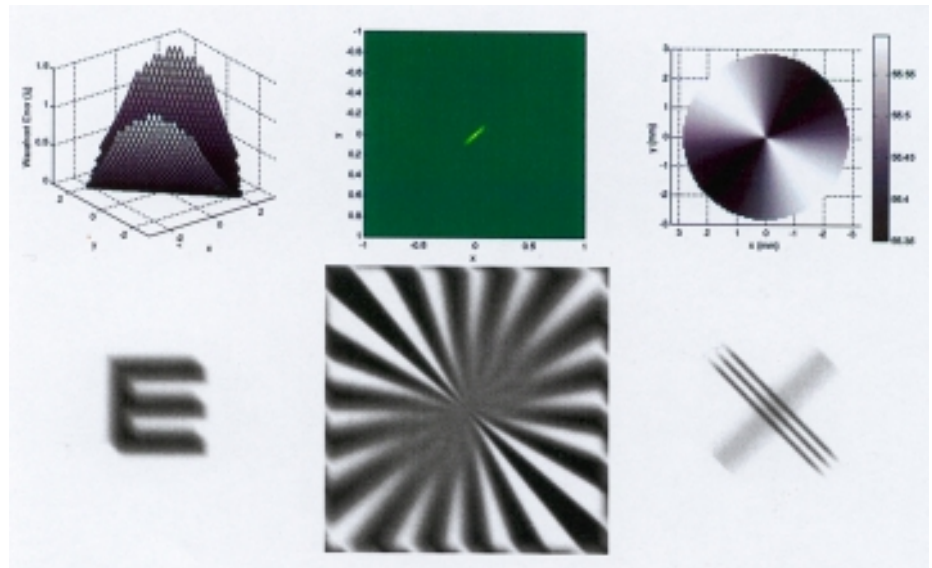


Figure 2. The effect of primary astigmatism on the retinal image. The top panel shows the wavefront error, the PSF, and the refractive power map. The values of the Zernike coefficients are chosen to be: $Z_0^0 = 0.125$, $Z_2^0 = 0.07$, $Z_2^2 = -0.1$. This corresponds to Seidel astigmatism of 0.5.

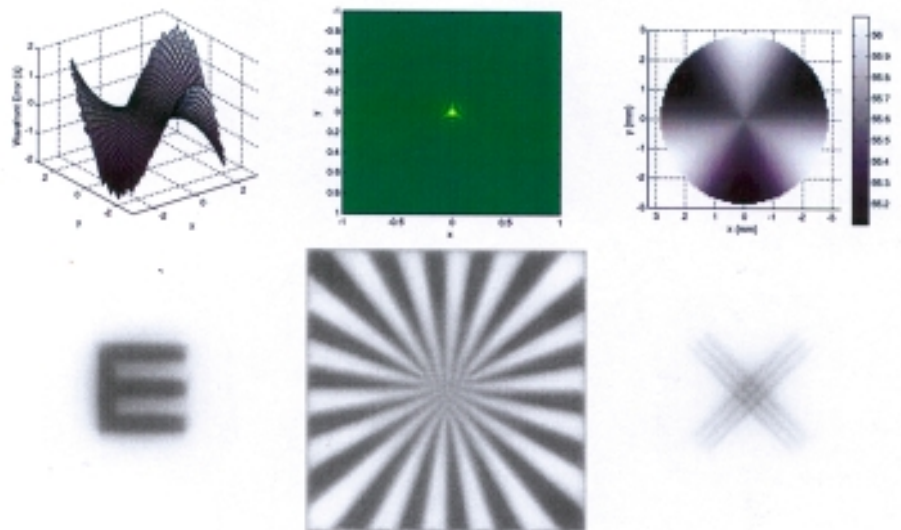


Figure 3. The effect of trifoil on the retinal image. The top panel shows the wavefront error function, the PSF and the refractive power map. The value of the Zernike coefficient is chosen to be: $Z_3^3 = -0.25$.

corresponds to defocus. It is a symmetric term which causes blur in all directions. The effect of defocus on retinal image is well reported and well understood. However, it should be noted that the classical Seidel defocus corresponds

to a combination of the fourth Zernike term and a balancing piston term.

The effect of higher-order aberrations

From the sixth Zernike term, we reach the

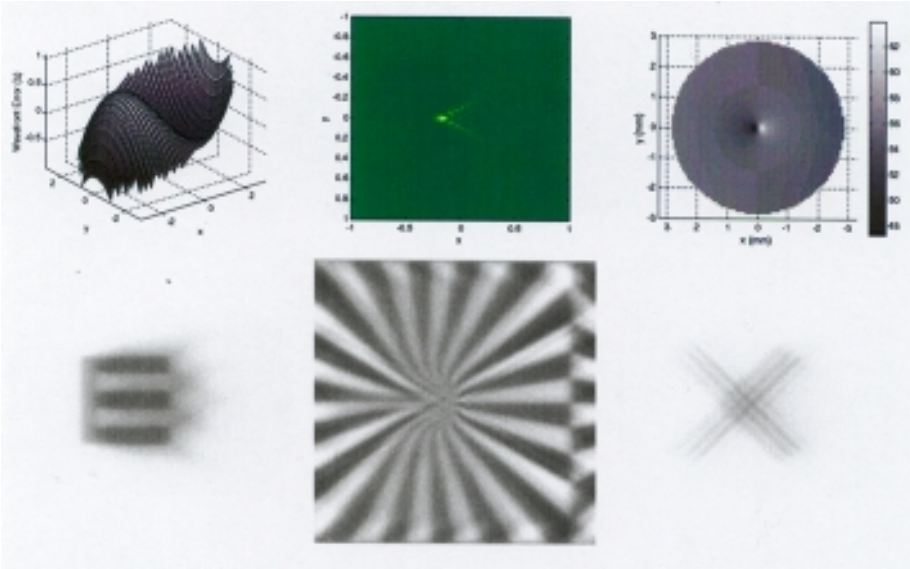


Figure 4. The effect of primary horizontal coma on the retinal image. The top panel shows the wavefront error function, the PSF and the refractive power map. The value of the Zernike coefficient is chosen to be $Z_3^1 = 0.25$.

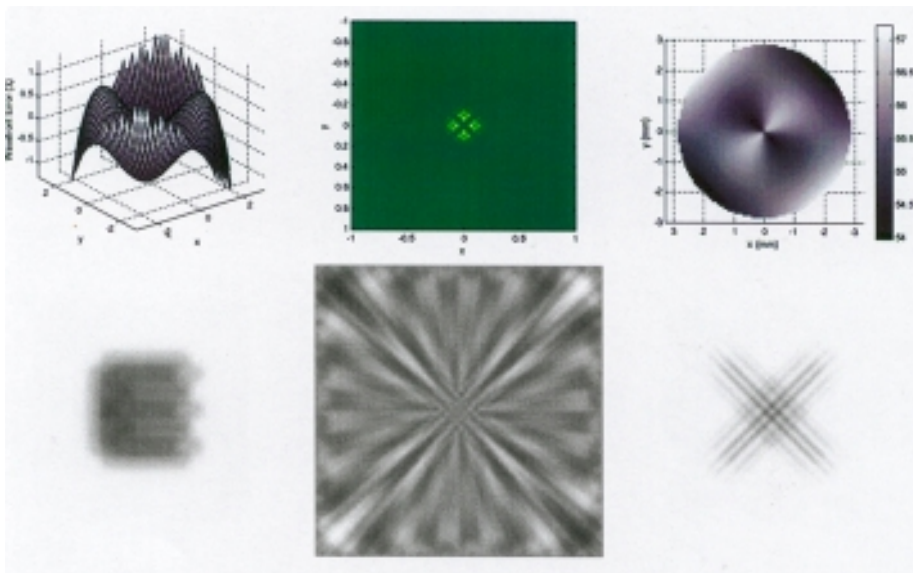


Figure 5. The effect of secondary astigmatism on the retinal image. The top panel shows the wavefront error function, the PSF and the refractive power map. The value of the Zernike coefficient is chosen to be: $Z_4^2 = -0.15$.

higher-order aberrations, which cannot be completely corrected with a traditional sphero-cylinder lens.

The sixth and ninth Zernike terms, $Z_3^3(\rho, \theta)$ and $Z_3^2(\rho, \theta)$, correspond to trifoil (three nodes in the wavefront). Trifoil

represented by the ninth Zernike term is rotated by 30 degrees with respect to the sixth Zernike term. In Figure 3, we show the effect of sixth Zernike term on retinal image. Although the appearance of trifoil on the retinal image can be mistaken for

defocus, the trifoil itself cannot be corrected with a sphero-cylindrical lens.

The seventh and eighth Zernike terms, $Z_3^1(\rho, \theta)$ and $Z_3^2(\rho, \theta)$, represent vertical and horizontal primary coma, respectively. The well-known coma defined by Seidel corresponds not only to the seventh or eighth Zernike terms but also to the combination of these terms with a prism term. The resulting retinal images are smeared along 90 to 270 degrees in the case of vertical coma and along 0–180 degrees in the case of horizontal coma. The sign of the coefficient determines the direction of smearing of the image. This leads to the horizontal component of the MTF being different from its vertical component. The meridional variations of the MTF are common for all higher order Zernike terms except the primary and higher-order spherical aberrations.

For example, a positive horizontal coma coefficient, as shown in Figure 4, smears the detail to the right, whereas a negative horizontal coma coefficient will smear the detail to the left. Note the image shift to the left clearly visible in the fan chart. That is why the seventh and eighth Zernike terms need to be balanced by a prism to represent pure coma. The effect of the seventh Zernike term is similar to the eighth term but in the y -axis.

The 10th and 14th Zernike terms, $Z_4^4(\rho, \theta)$ and $Z_4^2(\rho, \theta)$, represent tetrafoil (four nodes in the wavefront). The 14th Zernike term is rotated by 22.5 degrees with respect to the 10th Zernike term. The effect of tetrafoil on the retinal image is similar to trifoil. Again, as in the case of the trifoil, tetrafoil cannot be corrected with a spherical refractive correction.

The 11th and 13th Zernike terms, $Z_4^3(\rho, \theta)$ and $Z_4^1(\rho, \theta)$, represent secondary astigmatism. The 13th Zernike term is rotated by 45 degrees with respect to the 11th Zernike term. In the case of secondary astigmatism the PSF has four distinctive peaks and this corresponds to multiple images (polyopia) in the resulting retinal images as shown in Figure 5. The secondary astigmatism may be partially corrected with a cylinder lens.

The 12th Zernike coefficient, $Z_4^0(\rho, \theta)$, represents primary spherical aberration.

The effect of spherical aberration of the retinal image produces a symmetrical blur not unlike defocus. As in the case of astigmatism and primary coma, the well-known spherical aberration defined by Seidel corresponds not only to the 12th Zernike term but also to the combination of this term with balancing defocus and piston terms. In Figure 6, we show the effect of the 12th Zernike term on the retinal image. Note the symmetrical phase reversals (that is, light and dark bars reverse positions) in the centre of the fan chart typical for this kind of aberration.

Reconstruction of the retinal image for real eyes

To illustrate the effects of monochromatic aberrations on quality of the retinal image for real eyes, we have selected two subjects: subject A who has a decentered corneal apex and subject B who has undergone a poorly centred refractive surgery procedure.

We have chosen to illustrate the effects of corneal aberrations because they are of high amplitude for these subjects. This can be achieved by measuring the anterior surface of the cornea²³ and then deriving the optical aberrations using geometrical and wave optics.¹² In the past, computer-based raytracing techniques have been suggested for modelling visual performance of the cornea. As noted by Greivenkamp and associates,²⁴ such techniques were relatively simple to implement with commercially available software that was primarily designed for ophthalmic lens analysis. Recently, Guirao and Artal²⁵ have provided details on the methods, accuracy and limitations of deriving wavefront aberrations from corneal topography.

The corneal elevations for subjects A and B were measured by a videokeratoscope (Optikon Keratron). In Figure 7, we show the corneal axial power for subjects A and B. In our analysis we consider a 4 mm pupil diameter for subject A and a 3 mm pupil for subject B. It is assumed that the pupil is centred on the axis of the videokeratoscope. As previously, we consider first that the pupil transmittance function is modelled by a normative Stiles-

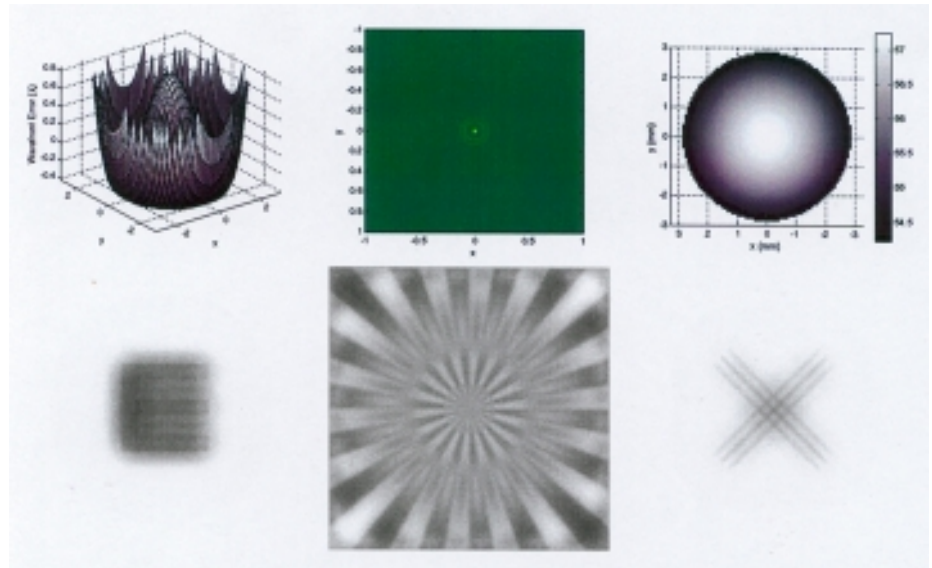


Figure 6. The effect of primary spherical aberration on the retinal image. The top panel shows the wavefront error function, the PSF and the refractive power map. The value of the Zernike coefficient is chosen to be: $Z_4^0 = 0.25$.

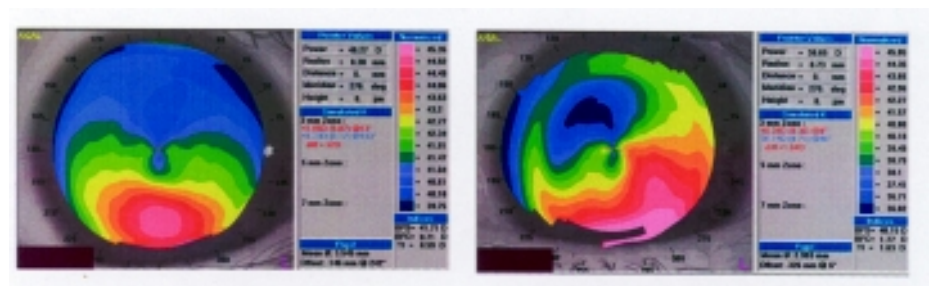


Figure 7. Corneal axial powers for subject A with decentered corneal apex (left) and subject B with decentered laser in situ keratomileusis (right)

Crawford function. Due to high corneal aberrations, we have assumed in the analysis, images of 100 mm by 100 mm positioned six metres from the pupil plane. Also, we have removed the effect of corneal spherical aberration, $Z_4^0 = 0$, assuming that it would be predominantly corrected by the natural spherical aberration of the crystalline lens.

The topography of subject A (Figure 7, left) shows a significant inferior decentration of the corneal apex. While this is similar to the topographic appearance of keratoconus, the axial power

values are within normal limits (39 to 45 D), suggesting simple downward displacement of the corneal apex. The optical effect of this decentration is similar to vertical coma. The wavefront, point spread function and refractive power map in Figure 8 all show a coma-like asymmetry along the vertical y -axis. The resulting retinal images show a distinctive downward smearing. This corresponds to high values of $Z_3^1(\rho, \theta)$ and $Z_1^1(\rho, \theta)$ in the Zernike representation of the wavefront error.

The case of subject B presents a more extreme example of higher order ocular

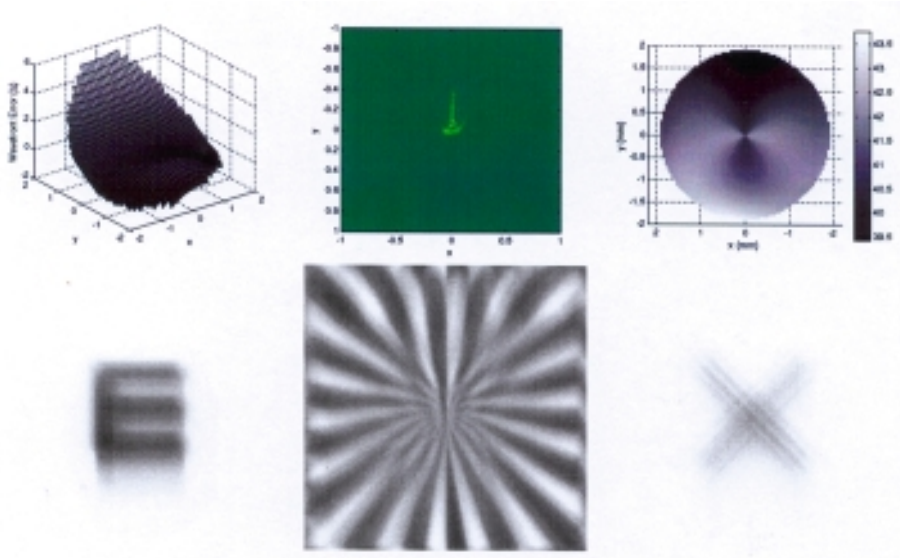


Figure 8. The effect of the corneal aberrations on the retinal image for subject A. The top panel shows the wavefront error function, the PSF and the refractive power map.

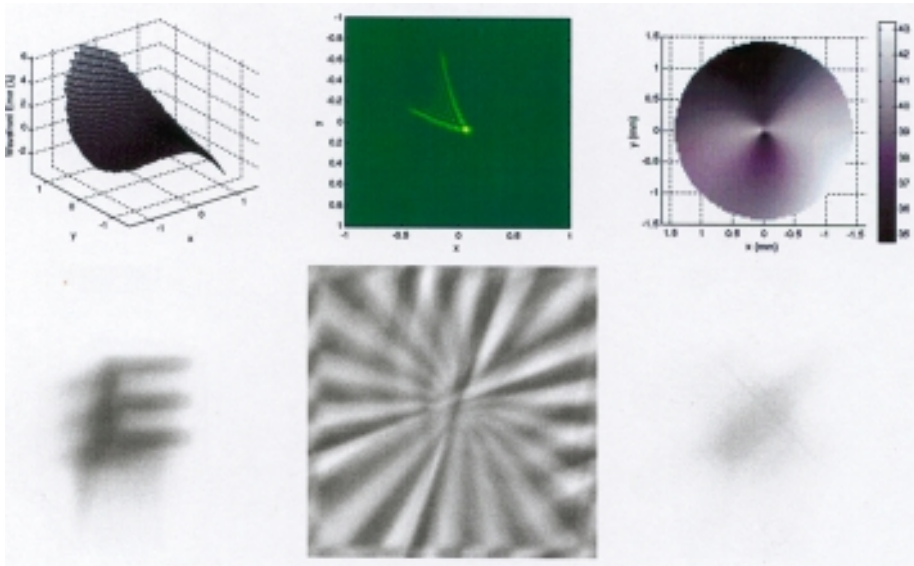


Figure 9. The effect of the corneal aberrations on the retinal image for subject B. The top panel shows the wavefront error function, the PSF and the refractive power map.

aberrations. The corneal topography of subject B (Figure 7, right) shows a flatter ablation zone, which is centred above and to the side of the pupil and geometric centre of the cornea. In Figure 9, the wavefront, point spread function and re-

fractive power maps illustrate a coma-like asymmetry at an oblique axis. The resulting retinal images show a marked smearing at an oblique angle down and to the left and a significant contrast loss. The images demonstrate substantial blurring and

loss of resolution of vertical detail. This is partly because of the increased magnitude of aberrations in subject B compared with subject A and partly because of the oblique angle of the primary aberrations in subject B. This corresponds to high values of $Z_3^1(\rho, \theta)$, $Z_3^3(\rho, \theta)$ and $Z_1^1(\rho, \theta)$, $Z_1^3(\rho, \theta)$ in the Zernike representation of the wavefront error.

CONCLUSIONS

There have been previous studies that relate ocular or corneal aberrations to image quality.²⁶⁻²⁹ Artal³⁰ performed image reconstruction on a single image for a number of emmetropic subjects and studied the effects of pupil size on retinal image quality while Greivenkamp and associates²⁴ used an image reconstruction algorithm to model visual acuity. Recently, image reconstruction has been used to simulate night vision in subjects after refractive surgery.³¹

The image reconstruction technique provides a powerful tool for investigating the quality of the retinal image. As the methods of measuring higher-order monochromatic aberrations of the eye with wavefront sensors become clinically viable, it should be possible to conduct real-time image reconstruction in the consulting room. This will provide the capacity for clinicians to better understand a patient's visual performance. The image reconstruction technique can broaden our knowledge of the effects of various forms of aberrations on retinal image quality for complex real-world scenes.

ACKNOWLEDGEMENTS

The authors wish to thank Ross Franklin, Jim Loughridge and Dion Scott for useful discussions and the anonymous reviewers for their constructive comments.

A Queensland University of Technology Seeding Grant supported part of this work.

REFERENCES

1. Howland HC, Howland B. A subjective method for the measurement of monochromatic aberrations of the eye. *J Opt Soc Am* 1977; 67: 1508-1518.

2. Walsh G, Charman WN. Measurement of the axial wavefront aberration of the human eye. *Ophthalmic Physiol Opt* 1985; 5: 23-31.
3. Atchison DA, Collins MJ, Wildsoet CF, Christensen J, Waterworth MD. Measurement of monochromatic ocular aberrations human eyes as a function of accommodation by the Howland aberroscope technique. *Vision Res* 1995; 35: 313-323.
4. Liang J, Grimm B, Goelz S, Bille JF. Objective measurement of wave aberrations of the human eye with the use of a Hartmann-Shack wave-front sensor. *J Opt Soc Am A* 1994; 11: 1949-1957.
5. Liang J, Williams DR. Aberrations and retinal image quality of the normal human eye. *J Opt Soc Am A* 1997; 14: 2873-2883.
6. Campbell MCW, Harrison EM, Simonet P. Psychophysical measurement of the blur on the retina due to optical aberrations of the eye. *Vision Res* 1990; 30: 1587-1602.
7. Salmon TO, Thibos LN, Bradley A. Comparison of the eye's wave-front aberration measured psychophysically and with the Shack-Hartmann wave-front sensor. *J Opt Soc Am A* 1998; 15: 2457-2465.
8. Williams DR, Brainard DH, McMahon MJ, Navarro R. Double-pass and interferometric measures of the optical quality of the eye. *J Opt Soc Am A* 1994; 11: 3123-3135.
9. Artal P, Marcos S, Navarro R, Williams DR. Odd aberrations and double-pass measurements of retinal image quality. *J Opt Soc Am A* 1995; 12: 195-201.
10. Stiles WS, Crawford BH. The luminous efficiency of rays entering the pupil at different points. *Proc R Soc B* 1933; 112: 428-450.
11. Wetherell WB. The calculation of image quality. In: Shannon RR, Wyant JC, eds. *Applied Optics and Optical Engineering*, Vol. VIII, Ch 6. London: Academic Press, 1980: 171-315.
12. Mahajan VN. *Optical Imaging and Aberrations: Ray Geometrical Optics*. SPIE Optical Engineering Press, 1998.
13. Collins MJ, Wildsoet CF, Atchison DA. Monochromatic aberrations and myopia. *Vision Res* 1995; 35: 1157-1163.
14. Noll RJ. Zernike polynomials and atmospheric turbulence. *J Opt Soc Am* 1976; 66: 207-211.
15. Thibos LN, Applegate RA, Schwiegerling JT, Webb R. VSIA Standards Taskforce Members. Standards for reporting the optical aberration of eye. (Cited 2000 Dec 1) Available from: UDL: <http://www.osa.org/Homes/vision/resources/into.htm>.
16. Conforti G. Zernike aberration coefficients from Seidel and higher-order power-series coefficients. *Optics Lett* 1983; 8: 407-408.
17. Tyson RK. Conversion of Zernike aberration coefficients to Seidel and higher-order power-series aberration coefficients. *Optics Lett* 1982; 7: 262-264.
18. Iskander DR, Collins MJ, Davis B. Optimal modeling of corneal surfaces with Zernike polynomials. *IEEE Trans Biomed Engin* 2001; 48: 87-95.
19. Walsh G, Charman WN. The effect of pupil centration and diameter on ocular performance. *Vision Res* 1988; 28: 659-665.
20. Applegate RA, Lakshminarayanan V. Parametric representation of Stiles-Crawford functions: normal variation of peak location and directionality. *J Opt Soc Am A* 1993; 10: 1611-1623.
21. He JC, Marcos S, Burns SA. Comparison of cone directionality determined by psychophysical and reflectometric techniques. *J Opt Soc Am A* 1999; 16: 2363-2369.
22. Marcos S, Burns SA. Cone spacing and waveguide properties from cone directionality measurements. *J Opt Soc Am A* 1999; 16: 995-1004.
23. Applegate RA, Howland HC. Noninvasive measurement of corneal topography. *IEEE Engin Med Biol Mag* 1995; 14: 30-42.
24. Greivenkamp JE, Schwiegerling J, Miller JM, Mellinger MD. Visual acuity modeling using optical raytracing of schematic eyes. *Am J Ophthalmol* 1995; 120: 227-240.
25. Guirao A, Artal P. Corneal wave aberration from videokeratography. *J Opt Soc Am A* 2000; 17: 955-965.
26. Hemenger R, Tomlinson A, Oliver K. Optical consequences of asymmetries in normal corneas. *Ophthalmic Physiol Opt* 1996; 16: 124-129.
27. Patel S, Marshall J, Fitzke FW. Model for predicting the optical performance of the eye in refractive surgery. *Refract Corn Surg* 1993; 9: 366-375.
28. Schwiegerling J, Greivenkamp JE, Miller JM, Snyder RW, Palmer ML. Optical modeling of radial keratotomy incision patterns. *Am J Ophthalmol* 1996; 122: 808-817.
29. Zhu L, Barttsch DU, Freeman WR, Sun PC, Fainman Y. Modeling human eye aberrations and their compensation for high-resolution retinal imaging. *Optom Vis Sci* 1998; 75: 827-839.
30. Artal P. Calculations of two-dimensional foveal retinal images in real eyes. *J Opt Soc Am A* 1990; 7: 1374-1381.
31. Schwiegerling J. Simulating retinal images following refractive surgery. In: *Vision Science and its Applications*, OSA Technical Digest (Optical Society of America, Washington DC, 1999) pp 250-253.

Author's address:

Dr D Robert Iskander
 Contact Lens and Visual Optics Laboratory
 Centre for Eye Research
 School of Optometry
 Queensland University of Technology
 Victoria Park Rd
 Kelvin Grove QLD 4059
 AUSTRALIA